Properties of the ultrashort gain length, self-amplified spontaneous emission free-electron laser in the linear regime and saturation

A. Murokh,[1] R. Agustsson,[1] M. Babzien,[2] I. Ben-Zvi,[2] L. Bertolini,[3] K. van Bibber,[3] R. Carr,[4] M. Cornacchia,[4] P. Frigola,[1] J. Hill,[3] E. Johnson,[2] L. Klaisner,[4] G. Le Sage,[3] M. Libkind,[3] R. Malone,[2] H-D. Nuhn,[4] C. Pellegrini,[1] S. Reiche,[1] G. Rakowsky,[2] J. Rosenzweig,[1] R. Ruland,[4] J. Skaritka,[2] A. Toor,[3] A. Tremaine,[3] X. Wang,[2] and V. Yakimenko[2]

[1]*UCLA Department of Physics and Astronomy, University of California at Los Angeles, 405 Hilgard Avenue, Los Angeles, California 90095-1547, USA*

[2]*Brookhaven National Laboratory, Upton, New York 11973, USA*

[3]*Lawrence Livermore National Laboratory, Livermore, California 94551, USA*

[4]*Stanford Linear Accelerator Center, Stanford, California 94309, USA*

(Received 13 December 2001; published 4 June 2003)

VISA (Visible to Infrared SASE Amplifier) is a high-gain self-amplified spontaneous emission (SASE) free-electron laser (FEL), which achieved saturation at 840 nm within a single-pass 4-m undulator. The experiment was performed at the Accelerator Test Facility at BNL, using a high brightness 70-MeV electron beam. A gain length shorter than 18 cm has been obtained, yielding a total gain of 2×10^8 at saturation. The FEL performance, including the spectral, angular, and statistical properties of SASE radiation, has been characterized for different electron beam conditions. Results are compared to the three-dimensional SASE FEL theory and start-to-end numerical simulations of the entire injector, transport, and FEL systems. An agreement between simulations and experimental results has been obtained at an unprecedented level of detail.

DOI: 10.1103/PhysRevE.67.066501 PACS number(s): 41.60.Cr, 41.60.Ap, 41.85.Ja

I. INTRODUCTION

There is a great interest in the scientific community towards development of the intense, short pulse, x-ray sources to probe the dynamics of chemical and biological processes at the molecular and atomic levels. In one promising scheme, it was suggested [1] to build an unseeded, single-pass, self-amplified spontaneous emission free-electron laser (SASE-FEL) based on the high brightness ultrarelativistic electron beam presently available at SLAC [2] and in the future at TESLA [3]. The concept of the SASE-FEL was introduced in the early 1980s [4,5], and in the following years the one-dimensional (1D) theory has been extended to include three-dimensional (3D) effects [6,7], and to describe temporal and statistical properties of the SASE radiation [8].

In recent years, with the advancement of the photoinjector technology [9], a series of successful experiments demonstrated high gain SASE operation, in the IR [10,11], visible [12], and ultraviolet [13] spectral ranges. Finally, a SASE-FEL saturation has been obtained [14] at 540 nm. The VISA (Visible to Infrared SASE Amplifier) experiment reported here was designed to further investigate the physical properties of the SASE-FEL relevant to the future LCLS operation. In particular, the efficiency limits of the SASE process were studied experimentally through optimization [15] of the undulator parameters for the best available low emittance photoinjector beam produced at the Accelerator Test Facility (ATF) [16]. VISA achieved saturation at 840 nm within a 4-m-long undulator with the SASE power gain length of 17.9 cm—more than a factor of 3 shorter than what had been previously achieved in this spectral range. The focus of this manuscript is on the measured FEL performance at the fundamental wavelength; while other results such as electron beam microbunching measurements and nonlinear harmonics generation are reported elsewhere [17,18].

II. EXPERIMENTAL SETUP

The general layout of the experiment is shown in Fig. 1. The ATF 1.6-cell photocathode *S*-band gun generated a high brightness electron bunch, which was accelerated in two consecutive SLAC-type linac structures to the VISA operating energy of around 71 MeV [19]. A 20° double-bend transport section served to direct the beam into Beamline III of the ATF experimental hall, where the VISA undulator was located.

The 4-m-long in-vacuum VISA undulator [20] was built at SLAC as a Halbach array of 220 periods, each 1.8-cm long. The pole magnets provided an on-axis peak field of approximately 0.75 T. In addition, the undulator was equipped with a periodic quadrupole lattice, which generated a strong focusing gradient throughout the length of the un-

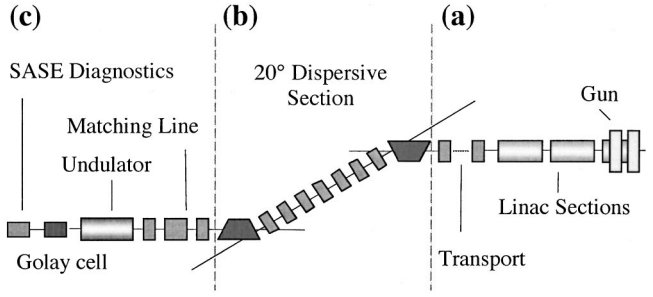

FIG. 1. Experimental layout of the ATF Beamline III: gun and linac area (a); 20° double-bend dispersive section (b); and VISA experimental area (c), including the undulator and radiation diagnostics.

dulator, forcing the electron beam matched β function to an average value of about 30 cm. The permanent magnet pieces were sorted to achieve field strength accuracy of better than 0.4%. The undulator structure was constructed out of four individual sections, each 0.994-m long. During the magnetic measurements performed at BNL [21], the quadrupole magnets were aligned and additional shimming was introduced to provide a desired central trajectory straightness [22] of better than 80 μm rms throughout each pair of the consecutive undulator sections. In order to align the magnetic axis of all four individual sections to better than 20 μm throughout the 4-m length of the device an interferometric alignment procedure was developed [23] and implemented at the location of the experiment. The undulator vacuum chamber was designed to allow an independent support and control to each undulator segment while in vacuum [24]; and a charge-coupled-device (CCD)-based optical monitoring system was developed [25] to trace the relative positions of the undulator sections with a 10-μm accuracy throughout the pumping cycles and if in-vacuum corrections were required.

The undulator and vacuum chamber design included eight diagnostic ports 50-cm apart, starting 25 cm into the undulator. The applications of these ports were both to measure SASE radiation properties along the undulator length, and to determine the electron beam position and envelope profile at three points throughout every betatron period. The undulator in-vacuum diagnostic probes were developed [26] to intercept the beam path inside the undulator during the measurements. To ensure clearance through 3.6-mm openings in the undulator frame the probes were constructed only 2.2-mm wide, which is nonetheless many times both the electron and radiation rms beam sizes. The active area of the probe—a double-sided silicon mirror—could be actuated in two positions: to reflect a FEL radiation into the optical diagnostic system, or to generate the optical transition radiation (OTR) for the electron beam imaging system, respectively. The polishing of these miniature mirrors to the laser quality surface finish presented a challenge, which motivated the use of silicon.

The initial design for electron beam diagnostic detectors considered single crystal YAG:Ce (where YAG is yttrium aluminum garnet) scintillating screens. However, a diagnostic test performed at the ATF indicated an intensity-dependent blooming of the beam image on the YAG screen with the electron beam parameters similar to the ones expected at VISA [26]. As an alternative, the OTR off the probe mirror surface, coupled with polarizers and filters to reject the SASE signal, was utilized to image the electron beam. The relatively low intensity of the OTR, coupled with the high optical noise environment inside the undulator, placed a significant limitation on the dynamic range of the OTR-based beam profile monitors [27]. Since beam trajectory control was one of the most technically challenging aspects of the experiment, a very stable fiber coupled reference diode laser was purchased and prealigned to the undulator magnetic axis with 20 μm accuracy, to provide a fiducial mark for the electron beam centeroid trajectory measurements.

TABLE I. Electron beam parameters and FEL performance for the noncompressed (case A) and compressed beam (case B), respectively.

	Case A	Case B
Electron beam energy	71.2 MeV	70.7 MeV
Beam charge, Q	250 pC	140 pC
Horizontal emittance, ε_n	2.1 ± 0.2 μm	3.3 ± 0.2 μm
Peak current, I_p	55 A	250 A
rms energy spread, $\Delta\gamma/\gamma$	$<0.10\%$	0.17%
FEL gain length, L_g	29.7 cm	17.9 cm
SASE wavelength, λ_r	831 nm	842 nm
No. of temporal spikes, M	4–5	1–2
Total gain, G	7×10^4	2×10^8

III. ELECTRON BEAM MEASUREMENTS

Initial measurements of the electron beam properties were performed at the exit of the linac (Table I). Emittance was determined with the quadrupole scanning technique, and optimized in the range of $\varepsilon_n\sim1.9-2.3$ μm. To determine the current profile, a calibrated linear energy chirping was applied to the electron beam and the horizontal beam profile was measured around the first bend of the dispersive section of the beamline. For a sufficient amount of chirp, the horizontal distribution was entirely dominated by the dispersion in the bend, and thus could be converted into the beam current profile. The measurement showed nearly flat top distribution with a peak value of about 55 A.

To achieve the design goals, however, a much larger beam current was required. This was achieved with the development of a bunch compression mechanism, utilizing second order effects in the dispersive section. Namely, the quadrupoles tune in the dispersive section was chosen such that the transport coefficient T_{566} was large and negative. As a result, the specific amount of the linac phase detuning resulted in the two effects: (1) the beam acquired a linear energy chirping in the linac ($\Delta\gamma/\gamma$); and (2) the initially small compression coefficient $R_{56}\approx T_{566}(\Delta p/p)$ increased to a significant value, as the beam centroid momentum was decreased by Δp. The combined effect, given the proper choice of the linac phase detuning and the beamline tune T_{566} values, resulted in a strong longitudinal bunch compression, and a much larger longitudinal current [28].

To measure the compression effect, a coherent transition radiation (CTR) diagnostics was implemented after the dispersive section of the beamline. The integrated intensity in the coherent fraction of the transition radiation spectrum generated by the electron bunch has a strong dependence on the bunch length σ_τ [29]. To measure the change of CTR intensity as a function of the linac phase detuning, the signal, generated by a 45° mirror intersecting the beam path after the dispersive section, was directed into a far-infrared bolometer. The measured CTR intensity (Fig. 2) showed a strong correlation with the linac rf phase, and thus allowed us to verify the compression process. In addition, an insertable low-pass filter with a known frequency roll-off was used for quantitative assessment of the high frequency CTR com-

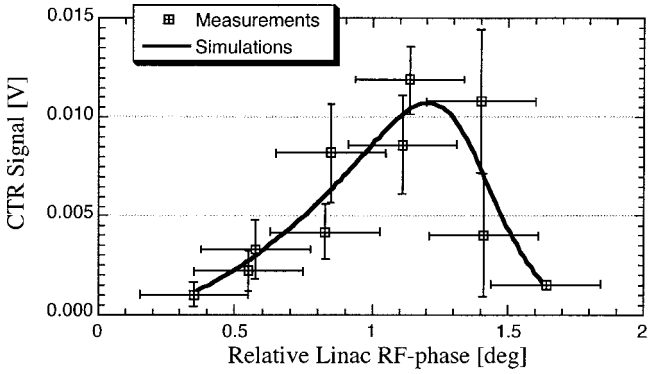

FIG. 2. Measured CTR signal intensity exhibits a sharp peak within a narrow window ($\sim$1.5°) of the linac RF phase.

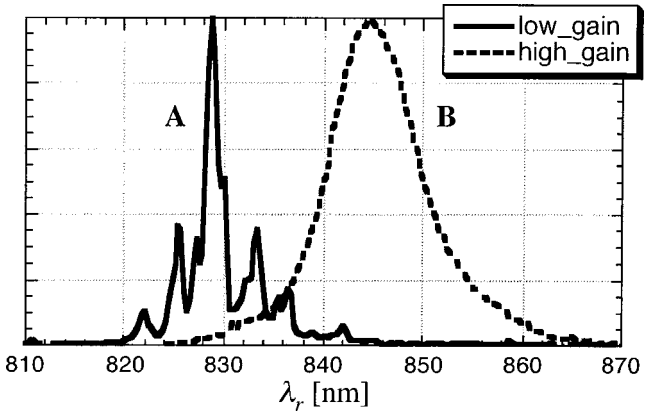

FIG. 3. Comparison of the SASE radiation spectra measured without (A) and with (B) compression. The spiky structure in case A indicates many longitudinal modes (i.e., a longer bunch length).

ponent. Measurements with and without the filter provided a benchmark for the numerical modeling of the system. As a result it was found that at the optimized value of the linac rf phase the bunch is compressed longitudinally by a factor of 5, yielding a peak current of 250 A.

IV. FEL MEASUREMENTS AND ANALYSIS

Without the bunch compression, VISA lased at 830 nm, with a SASE pulse energy of 5 nJ measured at the undulator exit, corresponding to a gain length of about 30 cm (Table I, case A). Spectral measurements [Fig. (3a)] showed a typical spiky structure, indicating the superposition of many temporal modes (spikes), as expected for a lasing core of the electron beam about 500-μm long [27]. With the compression in place [Fig. 3(b)], the spectrum was wider and lacked any structure, suggesting the single temporal mode [30], consistent with the shorter bunch length. With the compressed beam the SASE energy at the undulator exit increased by many orders of magnitude reaching up to 20 μJ and showing saturation when the optimized operating point was found.

Since the SASE process develops from a random shot noise in the electron longitudinal distribution, it was important to analyze the statistical properties of the FEL process, such as shot-averaged performance, and shot-to-shot fluctuations of the SASE intensity. However, that was not a trivial task since the bunch compression factor, being a strong function of the linac rf phase, was changing on the fast time scale, following the jitter in the rf system. As a result, the measured SASE fluctuations were strongly dominated by the linac rf noise. To overcome this problem, a collimator in the dispersive section was used to monitor the linac phase evolution by measuring the charge loss in the collimator. The nonlasing tale of the dispersion-dominated beam was clipped by the collimator, and the amount of clipping was monitored, allowing us to select for data analysis only those shots that were clipped by the same amount [26].

The shot-to-shot distribution of the SASE process depends on the number of independent lasing modes contributing to each shot and characterized with the Γ-function distribution [31]. In VISA the electron beam transverse size was typically only 60–90-μm rms, so that at the lasing wavelength the Raleigh range was much smaller than the gain length, and full transverse coherence was established early. As a result, the statistical properties of the intensity distribution were related entirely to the number of longitudinal spikes in the SASE radiation. In the absence of compression [Fig. 4(a)], a Γ-function fit indicated 4–5 temporal modes, and with the compressed beam, a distribution inside the undulator [Fig. 4(b)] resembled a negative exponential, characteristic of a single spike lasing [both distributions are consistent with the spectra in Figs. 3(a) and 3(b), respectively]. At saturation, however, the SASE intensity distribution from the compressed beam has changed dramatically [Fig. 4(c)], since it was no longer dominated by the shot noise fluctuations, but rather by the shot-to-shot fluctuations in the saturation length, which can be as large as few gain lengths for short bunches [30].

With the charge selection criterion described above, one could compare data sets obtained at the different diagnostic ports along the undulator, while the system stayed at the same operating point. As a result, the FEL gain evolution along the undulator length was studied. The measured intensity of SASE radiation had noticeably exceeded the level of a broadband spontaneous emission starting from the diagnostic port 3 (1.25 m into the undulator). In the curve shown in Fig. 5, the fit to the exponential part of the curve yielded a power gain length of 17.9 cm, corresponding to 3D FEL parameter $\tilde{\rho} \approx 0.0046$, reduced from the 1D limit by a factor

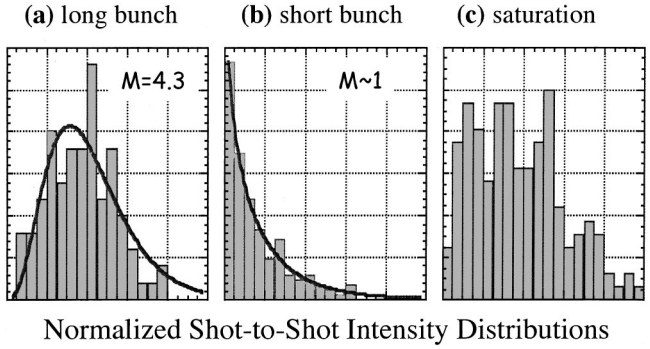

FIG. 4. SASE fluctuations (a) without compression and at high gain measured (b) inside the undulator and (c) at the undulator exit.

of $(1+\Lambda)\approx 1.75$, mostly due to diffraction. Near the undulator exit, the curve deviated from the exponential behavior, indicating saturation, which was quite consistent with the theoretical estimate of the saturation length [6], $L_{sat}\approx\lambda_u/\tilde{\rho}=3.9$ m.

The measured bandwidth at saturation, $(\Delta\omega/\omega)_f\approx 1.2\%$, was also found in agreement with the value predicted from theory, if one would add the contribution from the beam energy spread term: $\Delta\omega/\omega\approx 2\tilde{\rho}[1+2(\Delta\gamma/\gamma\tilde{\rho})^2]$. Finally, the SASE power at saturation was estimated to be about 75 MW based on the SASE energy and bandwidth measurements, which was consistent with the 3D scaling law $P_{sat}\sim 1.6P_{beam}\tilde{\rho}/(1+\Lambda)$ [32]. The final state SASE gain $G\equiv(dP/d\omega)_f/(dP/d\omega)_{noise}$ was evaluated using the treatment given in [33], using only the measured parameters:

$$G^{-1}\approx\frac{3\pi}{4}\left(\frac{K^2[JJ]^2}{1+K^2/2}\right)\frac{I_b}{I_A}\frac{m_ec^2}{P_f/k_rc}\left(\frac{\Delta\omega}{\omega}\right)_f\frac{\tilde{L}_g}{\lambda_u}.$$

With the undulator parameter $K=1.26$, and the average beam current over the spike length $I_b=210$ A, the gain value at saturation was found to be $G\approx 2\times 10^8$.

V. NUMERICAL MODEL OF THE EXPERIMENT

Since the details of the compression mechanism during the beam transport were critical for understanding the electron beam properties inside the undulator, a full cathode-to-undulator simulation of the experiment was needed to model the SASE results. Starting from the photoemission at the cathode, a UCLA version of PARMELA [34] was used to model acceleration and emittance compensation through the gun and linac sections. The PARMELA results matched the beam properties measured after the linac (Table I). The code ELEGANT [35] was used to model the beam dynamics and the bunch longitudinal compression in the double-bend dispersive section, including the effects of coherent synchrotron radiation (CSR). The beam compression was studied as a function of linac rf phase detuning, and the ELEGANT output should be tested against the CTR data (Fig. 2) to achieve a good agreement between a model and the experimental data over a wide range of system parameters. One critical result of the numerical simulations was understanding of the emittance growth mechanisms in the dispersive section. The ELEGANT CSR model showed that the slice horizontal emittance increase due to CSR was not significant, i.e., $\Delta\varepsilon_n^{CSR}\approx 0.3\ \mu$m rad. However, when the beam energy offset was set to model the maximum compression case, the noncompensated dispersion term, $\eta\sim 5$ cm, combined with the large slice energy spread in the compressed beam, dominated the emittance growth, bringing the effective horizontal slice emittance inside the undulator up to $\varepsilon_n^{\text{eff}}\approx 3.5\ \mu$m rad.

The 3D time-dependent code GENESIS 1.3 [36] was used to model the radiation evolution inside the undulator. An ELEGANT output file was converted into an input file for GENESIS preserving all 6D properties of the electron beam phase space [37]. The simulations of the FEL process are shown in Fig. 5 together with the experimental data. The measured SASE gain curve was well within the standard deviation of a set of GENESIS runs with randomly varying shot noise. In addition to a good agreement with measured SASE gain evolution, the developed numerical model accurately reproduced spectral and angular properties of the radiation. Figure 6 shows the hollow angular distribution of the SASE intensity measured at the exit of the VISA undulator, together with the one generated from the far field GENESIS output. Such an unusual SASE angular profile was repeatedly observed in the experimental measurements. It was reproduced numerically, when the strongly asymmetric and energy correlated horizontal phase space distribution in the electron beam, originated in the bunch compression process, was carried from the ELEGANT output into the FEL simulations. Having this unusual result reproduced with GENESIS indicated a new level of insight into the dynamics of the electron beam and SASE FEL systems, obtained by the synthesis of copious diagnostic measurements and rigorous, detailed simulations.

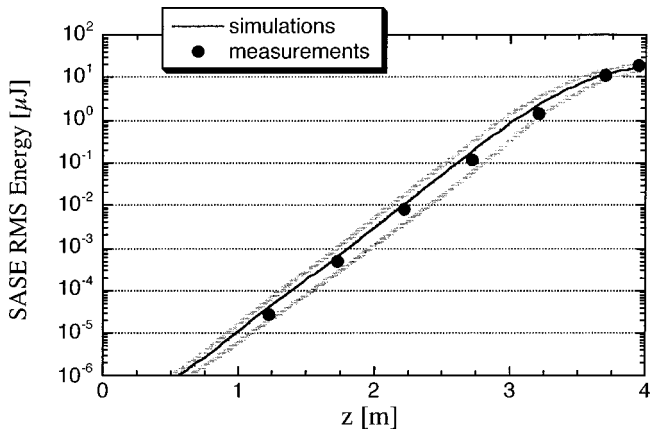

FIG. 5. Measured SASE evolution along the undulator length and numerical simulations (gray lines are the rms boundaries of the set of GENESIS runs). The amplification curve yields power gain lengths of 17.9 cm and saturates near the undulator exit.

In conclusion, the VISA experiment presented an extensive study of the dynamics of a high gain SASE FEL driven by a high brightness, longitudinally compressed electron beam in a strong focusing, compact undulator. A gain of 2×10^8 and saturation were obtained, and the statistical properties of the SASE signal at saturation were measured. SASE evolution as well as spectral and statistical properties of the radiation were measured and found to be in good agreement

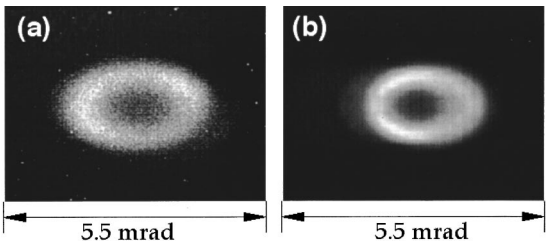

FIG. 6. Far field angular distribution of the SASE radiation (a) measured on the CCD camera and (b) simulated with GENESIS.

with the 3D FEL theory. To explain fine details in the performance of the system, it was necessary to investigate, both experimentally and through numerical modeling, the dynamics of the electron beam throughout the entire injector-transport-FEL process. The developed start-to-end integrated computational model showed an excellent agreement with the measurements, and gave strong insights into the physical mechanisms of the complex phenomena present in the experimental system.

ACKNOWLEDGMENT

This work was done under DOE Contract No. DE-FG03-92ER40693.

[1] C. Pellegrini, Proceedings of the Workshop on 4th Generation Light Sources, SLAC, 1992 (unpublished).
[2] Linear Coherent Light Source Design Study Report No. SLAC-R-521, 1998 (unpublished).
[3] Linear Collider Conceptual Design Report No. DESY 97-48, 1997 (unpublished).
[4] R. Bonifacio, C. Pellegrini, and L. Narducci, Opt. Commun. **50**, 373 (1984).
[5] A. M. Kondratenko, E. L. Saldin, Part. Accel. **10**, 207 (1980).
[6] K. J. Kim, Phys. Rev. Lett. **57**, 1871 (1986).
[7] S. Krinsky and L. H. Yu, Phys. Rev. A **35**, 3406 (1986).
[8] R. Bonifacio *et al.*, Phys. Rev. Lett. **73**, 70 (1994).
[9] J. S. Fraser *et al.*, IEEE Trans. Nucl. Sci. **32**, 1791 (1985).
[10] M. Hogan *et al.*, Phys. Rev. Lett. **80**, 289 (1998); **81**, 4867 (1998); D. C. Nguyen *et al.*, *ibid.* **81**, 810 (1998).
[11] L. H. Yu *et al.*, Nucl. Instrum. Methods Phys. Res. A **445**, 301 (1999); Proceedings of the FEL Conference 2000, Duke University (2000).
[12] M. Babzien *et al.*, Phys. Rev. E **57**, 6093 (1998).
[13] J. Andruszkow *et al.*, Phys. Rev. Lett. **85**, 3825 (2000); V. Ayvasyan *et al.*, *ibid.* **88**, 104802 (2002).
[14] S. V. Milton *et al.*, Phys. Rev. Lett. **85**, 988 (2000); Science **292**, 2037 (2001).
[15] H.-D. Nuhn (private communication).
[16] X. Wang, X. Qiu, and I. Ben-Zvi, Phys. Rev. E **54**, 3121 (1996).
[17] A. Tremaine *et al.*, Phys. Rev. Lett. **88**, 204801 (2002).
[18] A. Tremaine *et al.*, Phys. Rev. E **66**, 036503 (2002).
[19] X. Wang *et al.*, *PAC 1999 Proceedings*, edited by A. Luccio and W. MacKay (IEEE, Piscataway, 1999), p. 3495; V. Yakimenko *et al.*, FEL 2001 Proceedings (unpublished), p. 277.
[20] R. Carr *et al.*, Phys. Rev. ST Accel. Beams **4**, 122402 (2001).
[21] G. Rakowsky *et al.*, *PAC 1999 Proceedings*, edited by A. Luccio and W. MacKay (IEEE, Piscataway, 1999), p. 2698.
[22] P. Emma and H. D. Nuhn, *FEL 1998 Proceedings* (Elsevier Science B.V., Amsterdam, 2000), Vol. II, p. 35.
[23] R. Ruland *et al.*, *PAC 1999 Proceedings*, edited by a. Luccio and W. MacKay (IEEE, Piscataway, 1999), p. 1390.
[24] M. Libkind *et al.*, *PAC 1999 Proceedings*, edited by A. Luccio and W. MacKay (IEEE, Piscataway, 1999), p. 2477.
[25] A. Tremaine, A. Murokh, and X. Wang, BNL Report No. 68170, 2001 (unpublished).
[26] A. Murokh *et al.*, *PAC 2001 Proceedings*, edited by P. W. Lucas and S. Webber (IEEE, Piscataway, 2001), pp. 2748 and 1331.
[27] A. Murokh, Ph.D. thesis, UCLA, 2002.
[28] J. B. Rosenzweig (private communication).
[29] A. Murokh *et al.*, Nucl. Instrum. Methods Phys. Res. A **410**, 452 (1998).
[30] R. Bonifacio *et al.*, Phys. Rev. Lett. **73**, 70 (1994).
[31] E. L. Saldin *et al.*, Opt. Commun. **148**, 383 (1998).
[32] M. Xie, PAC 95 Proceedings (unpublished), p. 183.
[33] L. H. Yu and S. Krinsky, Nucl. Instrum. Methods Phys. Res. A **285**, 119 (1989).
[34] E. R. Colby, Ph.D. thesis, UCLA, 1997.
[35] M. Borland, Advanced Photon Source Report No. LS **287**, 2000 (unpublished).
[36] S. Reiche, Nucl. Instrum. Methods Phys. Res. A **429**, 243 (1999).
[37] S. Reiche (private communication).